A Scheme For Gravitational Wave Detection With Modified Space-Hypertelescope

Rijuparna Chakraborty

Department of Electronics and Communication Engineering, Institute of Engineering and Management, India

Email: rijuparna.chakraborty@iem.edu.in

Abstract. *Context*: Hypertelescope is a promising astronomical multi-aperture telescope that can render very high-resolution direct images of deep sky objects. A space version of this system can easily provide 0.1 microarcsecond resolution in visible wavelength range. *Aim*: To study the feasibility of using Space-based-Hypertelescope as Gravitational Wave detector. *Method*: The study was carried out by calculating the responsivities of the system along with its sensitivities over a broad frequency range. For sensitivity calculation we relied upon the available data of noise power spectral densities of other space-based systems. *Results*: It came out that some modification in the structure is necessary in order to reduce the radiation pressure noise on the mirrors as well as its spring constant. A detector with super-resolution capacity will be preferable for the suggested configuration. *Conclusion*: We present a modified Space-Hypertelescope system that can work as gravitational wave detector for frequencies more than 1Hz.

INTRODUCTION: ASTRONOMICAL TELESCOPES

Since ancient days of civilization astronomers had used their study on the movements of planets and stars to make an accurate calendar, to understand seasonal changes and tidal behaviors. Telescope added a great tool to their studies. Although it is not clear who made the first telescope, but Galileo successfully used it to study the heavenly bodies and documented their properties. The introduction of reflective telescope by Newton solved many problems related to aberration and increased the telescope resolution by several orders. The study of deep sky objects got even more thrust with the advent of multi-aperture telescope concept. Telescopes working in visible light range and radio frequency range started studying those objects quite efficiently. It enabled astronomers to search for habitable exo-planets, as well as the evolution of universe. This study got a new dimension in recent years with successful introduction of gravitational wave detectors. These detectors are fundamentally different from the typical astronomical telescopes in the sense that they use laser light interferometry to detect gravitational strain instead of gathering star-light. It can be said that these detectors ‘can hear’ but ‘cannot see’ our universe! Therefore, it would be a good idea to have both the abilities within one system. In other words, we would like to have a gravitational wave detection system within a star-gazing telescope.

Current GW detectors, such as LIGO, Virgo, KAGRA, and as well as the upcoming space-based GW detector LISA basically use Michelson-Morley type interferometer containing a Fabry-Perot cavity in its perpendicular arms. Therefore, they use temporal coherence for the interferometry. On the other hand, the multiple aperture astronomical telescopes use spatial interferometry – the bigger the distance between two apertures, the greater the resolution. The principle behind detecting GW in such a telescope lies in the detection of momentary deflection and perturbation of star images due to the passing of a GW. SIGN and Hypertelescope are two strong contenders in this field. The details of the SIGN scheme have been described by Park et. al. in several articles since 2019, whereas the basic concept of Hypertelescope was introduced by Labeyrie in 1996 and the design of its space version was proposed by him in 2010. Later Labeyrie et. al. published a whitepaper on Space-based Hypertelescope Observatory Scheme in 2013. Here in this present article we are to inspect if such a Space Hypertelescope can be used for GW detection simultaneously while studying deep-sky objects.

MODIFIED HYPERTELESCOPE

Hypertelescope is a multiple aperture telescope, whose apertures are distributed on a spherical or paraboloidal structure. These apertures are plane mirrors, and collectively they construct the primary mirror M1. The starlight is collected at the focus of this primary mirror and sent to the pupil densifier part through the relay optics for further processing. Therefore, the basic information collection is done by the array primary mirror and the collector at its focus, and if there be any changes due to the passing of any gravitational wave (GW), that will affect the wavefronts reaching this primary mirror.

In his book-chapter on Hypertelescope in Space, (2018) Labeyrie presented an intriguing scheme for placing, holding and adjusting primary mirror positions in space, using optical tweezers. The small flat shaped sub-aperture mirrors were to be trapped by a pair of laser beams, actually derived from same laser. This laser was supposed to be tunable and varying the wavelengths of the laser the mirrors were to be placed on a proper paraboloidal locus.

Although the scheme is fascinating, but its implementation may be difficult in several ways. First, due to the large size of the Hypertelescope, the trapping laser beam will have to travel a very long distance. Deriving two trapping beams from the same one, will make the distance even longer, and thereby requiring an extremely high-power laser as well as very large focusing optics. Secondly, the optically trapped mirrors may produce very high amount of noise at the collecting optics in the optical wavelength range itself. Moreover, the stiffness of optical tweezers will restrict it to be used for GW detection, which requires a free-falling condition.

In order to overcome these difficulties here we propose a slightly modified scheme. The suggested scheme is described below in Figure 1.

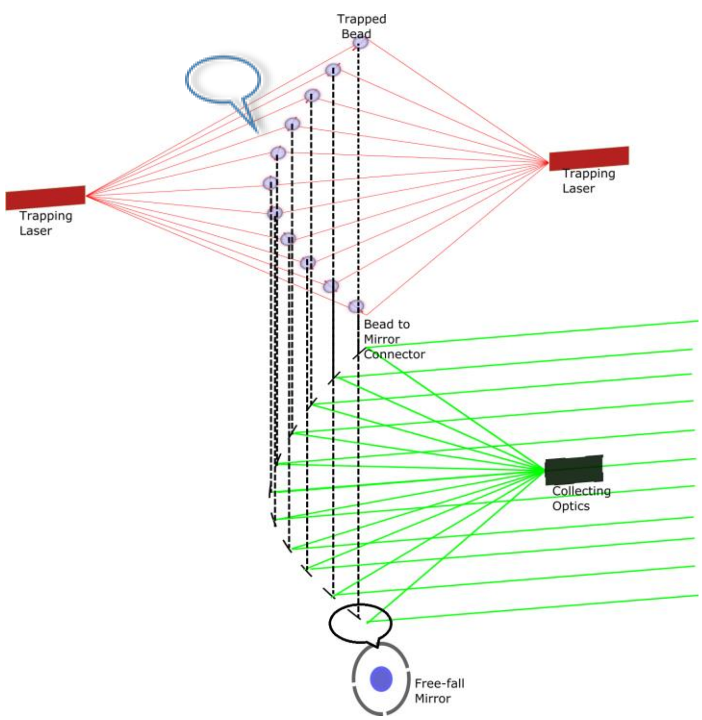

Figure 1. The schematic representation of the modified three-satellite Hypertelescope structure, where the satellites carry the trapping lasers and collecting optics. The two trapping lasers trap some optically transparent objects (filled circles), which carry the mirror sub-apertures placed in parabolic fashion through the small connectors (shown in black dotted lines). The star-light (in green) gets reflected by the mirrors towards the collecting optics. The scales in this representation is highly skewed – the length of the connectors will actually be far smaller than the distances travelled by all the light beams.

We propose a three-satellite Space-Hypertelescope structure - two satellites carrying two phase locked trapping laser on-board and the third carrying the collecting optics within it. The use of two separate lasers for trapping purpose will reduce the distance travelled by the beams, and also make its focusing easier.

Now, instead of trapping the mirrors directly, here we propose to trap some optically transparent objects, which are connected to the mirror housings by a multistage-spring attachment. The connector does not need to be very long, may be around one meter, in a proper direction so that the detector optics remain free from reflected-laser noise. Along with this, it has to be ensured that the centre of mass of the total trapped object remains in the trapping centre. Also, we propose to place the mirrors within their housings in free-fall conditions by using similar electrostatic positioning technology used by LISA, or by using comparable magnetic arrangement. This structure will decouple the mirrors from tweezers noise and will make it ready for GW detection.

The dimension of the telescope

In order to calculate the sensitivity of such a system, it is important to have the idea of its size. This will depend upon our targeted celestial object, as well as our beam combining technology. The size will also be limited by the optical trapping ability of the laser at large distances and angles.

Here for our target object, we consider Crab Pulsar, which has radius R=10 km, apparent magnitude m=16.5, luminosity 0.9 $L_\odot$ and distance d=7,175 light years.

The fluxes and magnitudes of the stars are generally calculated in the reference to some standard star using the realation

$$m_1 - m_{ref} = -2.5 \log_{10}\left(\frac{F_1}{F_{ref}}\right) \tag{1}$$

In terms of the attainable flux, the reference V = 0 star has a monochromatic flux of $F_\lambda = 3.61 \times 10^{-11} W$ $m^{-2}\ nm^{-1}$. These numerical values were collected from webpage of Dhillon *et. al.*.

Therefore, putting $m_{ref} = 0$ and $F_{ref} = 3.61 \text{ x } 10^{-11}\ W\ m^{-2}\ nm^{-1}$, we get $F_1 = 3.61 \text{ x } 10^{-17.6} W\ m^{-2}\ nm^{-1}$

Therefore, light flux reflected by one mirror of diamerer $a = 15cm$ will be $F \sim 6.4 \times 10^{-19}$ W. This will be distributed over a larger circular area due to diffraction. At distance S, the diameter of that area can be calculated as $w_S = \frac{\lambda S}{a}$. This power will be collected by the sensor of diameter a_s.

Therefore, for Fizeau type telescope, which combine these beams without beam expander, we get the received power $F_1 \times \left(\frac{a}{w_S}\right)^2 \times \pi \left(\frac{a_s}{2}\right)^2$

For simplicity we consider $a_s = a$.

In case of Hypertelescope, with the presence of pupil densifier we get a high gain in power depending upon the densification factor $\gamma_d = \left[\frac{d_o}{D_o}\right] / \left[\frac{d_i}{D_i}\right]$, where d and D are the aperture sizes of sub-apertures and array aperture. i denotes the entrance pupil and o denotes the exit pupil. The densifier intensifies the image by a factor of γ_d^2. For a completely filled pupil, and for $N \times N$ sub-apertures arranged on square grid pattern we can write, $\gamma_d = \frac{D_i}{N d_i}$.

For other technical considerations we keep the sub-aperture diameter fixed to 15cm. For entrance pupil diameter ~1000km, for mirrors in square-grid with 100 apertures in a row, we get the gain ~4.4×10^9. If we consider just a row configuration of the mirrors, we get a densification in the order of 6.6×10^4. With this gain we get the power output ~ $1.8 \times 10^{-17} W$, for one aperture One photon of 550nm has power ~ $3.61\ x\ 10^{-19}\ W$. (Without densification the output power becomes ~ $2.6 \times 10^{-22} W$). Therefore, we get ~50 photons, and collectively around 5000 photons. For 500km aperture, on the other hand without densification we get the output power ~ $3.6 \times 10^{-17} W$, while with densification it becomes ~ $10^{-11} W$, which is much better than 1000km scheme. But in that case, we are bound to lose our resolution.

Here, our present purpose is to increase the resolution of the telescope in order to detect the small strains developed by GW. For the strain h developed by a passing gravitational wave, the maximum change in length between two points separated by a distance S, will be hS. Therefore, if the collecting optics be at a distance comparable to S, the angular change will be of the order of h - which amounts around 10^{-21} for high frequency region. The question arises can Hypertelescope detect such a small angular change?

For a normal telescope with the highest baseline $D = 1000km$, the highest angular resolution becomes $\lambda/D \approx 5.5 \times 10^{-13}$ for 550nm wavelength. Here we recall that for pupil densified Hypertelescope, the peak of the PSF function moves γ_d times faster than the Airy envelop, where γ_d is the densification factor. Therefore, an angular change of 10^{-21}, will be magnified by this factor, giving the final angular change of the order $\sim 10^{-16}$. By changing the number of mirrors and by placing the apertures wisely over the parabolic locus the angular magnification can be increased by another order.

Unfortunately, it is still two to three orders lower than the highest resolution – considering single dimensional arrangement. This gap can be bridged up using the newly invented technology of super-oscillation, which may improve “the efficiency by three orders of magnitude” (Zheludev et. al. 2022, Rogers et. al. 2018)! This technique necessitated some additional set up at the detector side, which has to be designed according to the requirement. Moreover, for square-grid formation of the mirrors, the two dimentional fringes will go through a sudden overall rotation, which should be easily detectable.

Here we would like to mention that for an appropriate source, in future years Hypertelescope may span even over 10000km, and in that case no additional set-up will be required to detect such vibrations. However, here we limit ourselves to 1000km keeping in mind the available photon limit, the required resolution and also the laser trap controls.

Sensitivity of Hypertelescope to Gravitational Wave

The transit of a GW affects the space-time curvature, and the space gets periodically compressed and rarefied because of it, more like a longitudinal wave. Here we note the GW is transverse in nature and the change in space happens in the perpendicular direction of the GW propagation.

Now let us consider the Hypertelescope system is getting affected by a GW, generated by an inspiraling binary system comprising of two stars or black holes, each having mass M, angular frequency ω_{GW} and radius of inspiral circle is R. Then the magnitude of strain at a distance r from that centre, oscillates as a function of time t approximately as (Brilliant website, Carroll (chapter 7))

$$h = \frac{8GM}{rc^4} \omega_{GW}^2 R^2 \cos\left(2\omega_{GW}(t - r/c)\right) \tag{2}$$

where, gravitational constant $G = 6.6743 \times 10^{-11}$ m^3 kg^{-1} s^{-2}. For crab pulsar $M = 6.6743 \times 10^{30}$kg

and $R = 10$ km and the distance to Earth r is 7,175 light years.

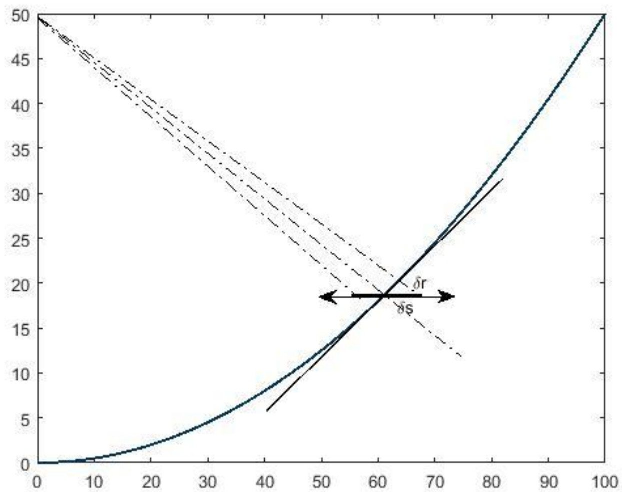

Figure 2. Dispacement direction of Hypertelescope mirror.

Now, let us denote the distance of the receiver from the inspiral centre by r_0 and the distance of the (i, j)th sub-aperture by $r_{i,j}$.

Also let us consider the directions of both star light and GW are parallel to the paraboloid axis – which is the vertical axis here. Due to the GW the sub-aperture mirrors will oscillates horizontally. In normal condition, i.e. without GW, the starlight with plane wavefront, will hit the apertures mirrors and will get reflected to the focus simultaneously, towards the receiving optics. But due to GW the phase of each reflected beam will change.

The sub-aperture at $r_{i,j}$ will change position by

$$\Delta S_{ij} = \frac{8GM}{r_{ij}c^4}\omega_{GW}^2 R^2 \cos\left(2\omega_{GW}\left(t - \frac{r_{ij}}{c}\right)\right) \tag{3}$$

Here we note that, this change in position is expressed in terms of the coordinate fixed at the GW source. And with respect to that source the position of the receiver too will change by

$$\Delta S_0 = \frac{8GM}{r_0 c^4}\omega_{GW}^2 R^2 \cos\left(2\omega_{GW}\left(t - \frac{r_0}{c}\right)\right) \tag{4}$$

Therefore, the net change in position of the sub-aperture with respect to the receiver will be

$$\delta S_{i,j} = \Delta S_{ij} - \Delta S_0 \tag{5}$$

i.e.,

$$\delta S_{ij} = \frac{8GM}{c^4}\omega_{GW}^2 R^2 \left[\frac{1}{r_{ij}}\cos\left(2\omega_{GW}\left(t - \frac{r_{ij}}{c}\right)\right) - \frac{1}{r_0} cos\left(2\omega_{GW}\left(t - \frac{r_0}{c}\right)\right)\right] \tag{6}$$

Now, considering $r_0 \gg |r_{ij} - r_0|$, and $|r_{ij} - r_0| = l_{ij}$, we can write

$$\delta S_{ij} = \frac{8GM}{r_0 c^4} \omega_{GW}^2 R^2 \left[\sin\left(\frac{\omega_{GW}}{c}(ct - l_{ij}\right) sin\left(\frac{\omega_{GW}}{c} l_{ij}\right)\right] \tag{7}$$

Let us consider the (i,j)th mirror is lying on the parabola described by the equation $y = ax^2$. If the focal length of the parabola be b, then we can write $y = x^2/4b$. For such a system the distance between receiver and mirror at (x, y) will be $l = \frac{(x^2+4b^2)}{4b}$, and the slope of the tangent will be $\tan\theta = \frac{x}{2b}$. For the receiver at focus of the parabola, i.e. at the location $(0, b)$, the maximum span of the mirrors can be denoted by x_{max}. The condition for receiving light at focus will be $y_{max} \leq b$, which gives $x_{max} \leq 2b$, and $\theta_{max} = 45°$. Now due to change in position, the new distance become $l \pm \delta l = \sqrt{(x \pm \delta S)^2 + \left(b - \frac{(x\pm\delta S)^2}{4b}\right)^2}$

Therefore, the change in length will be $\delta l = \frac{\delta S(2x\pm\delta S)}{4b} \approx \delta S \frac{x}{2b}$, assuming $x \gg \delta S$. Consequently, the change in phase added for each sub-aperture can be expressed as $\delta\phi = \frac{2\pi}{\lambda}\delta l$.

Therefore, the total phase difference for N apertures can be expressed as $\Delta\phi = \sum_N \delta\phi_{i,j}$

$$\Delta\phi = \frac{2\pi}{\lambda}\frac{x}{2b}\frac{8GM}{r_0 c^4}\omega_{GW}^2 R^2 \sum_N \left[sin\left(\frac{\omega_{GW}}{c}(ct - l_{ij}\right) sin\left(\frac{\omega_{GW}}{c} l_{ij}\right)\right] \tag{8}$$

The responsivity will be represented by

$$\sqrt{\mathcal{R}} = \sum_N \left[sin\left(\frac{\omega_{GW}}{c}(c\tau - l_{ij}\right) sin\left(\frac{\omega_{GW}}{c} l_{ij}\right)\right] \tag{9}$$

Now considering the integration time of this system (τ) corresponds to the time of flight for light from the farthest sub-aperture to the receiver, we can write $c\tau = x_{max}$.

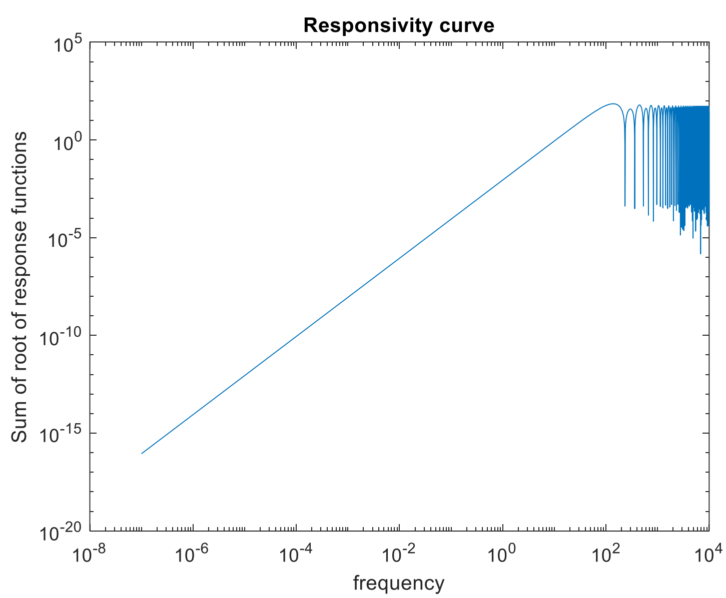

Figure 3. Responsivity curve for space based Hypertelescope with 1000km span

THE SENSITIVITY CURVE

The sensitivity curve indicates the minimum signal power $P(f)$ needed to overcome the total existing noise power $P_n(f)$ in order to detect the presence of GW. Now, the response of the system varies with signal frequency besides the noise power spectral density. The system sensitivity represents the combined effect of these two factors. "As such, it might have been more logical to have this (the responsivity) multiplying the signal power, but early on, it was decided to apply the inverse of this factor to the noise power to define a sensitivity curve—c'est la vie." (Robson et. al.)

Therefore, the sensitivity, i.e. the strain spectral density is defined as

$$S_n(f) = \frac{P_n(f)}{R(f)} \tag{10}$$

Now, this noise spectral density depends on various noise sources. For LISA, the main noise contributions come from Optical Metrology Noise, Test Mass Acceleration noise (P_{acc}) and Optical Path Noises (P_{OPN}).

The optical metrology noise is system specific and defines the primary nature of the sensitivity curve. Here we are concerned about the power coming from the target stellar source, which is getting affected by the passing GW. The GW will modulate it sinusoidally. Therefore, the power affected by GW can be represented as $P_{GW} = P_0\,[sin(\phi_0 + \Delta\phi)]^2 \approx P_0|\sin 2\,\phi_0|\Delta\phi$

Now let us consider that the wave reaching the telescope is getting modulated by a passing GW. The integration time of the system is τ, the average power reaching the detector during that period is P_0 and the number of photons carrying that power is n. The wavelength of the light is λ and the angular frequency is ω. Then the power collected within that period can be expressed as $P = \frac{n\hbar\omega}{\tau}$. Its variation can be calculated using Poisson's distribution of photons $\Delta n = \sqrt{n}$, which gives $P_n(\omega) = \sqrt{n}\frac{\hbar\omega}{\tau} = P/\sqrt{n}$.

Following the strain sensitivity ($\sqrt{S_n(f)}$) analysis of Park *et. al.*, we relate it with the signal to noise ratio (SNR) by

$$SNR = \, h|_{max}\sqrt{\frac{\tau}{S_n(f)}} = \frac{P_{GW}}{P_n} \tag{11}$$

where, $h|_{max}$ is the GW signal amplitude, and τ is the integration time, which can be expressed as $\tau = 1/f$.

Therefore, we get

$$\sqrt{fS_n(f)} = \frac{h|_{max}}{SNR} = \frac{h|_{max}\,P_n}{P_{GW}} = h|_{max}\,\frac{P/\sqrt{N}}{P_0|sin\,2\phi_0|\Delta\phi} \tag{12}$$

From this expression too, we find that

$$\sqrt{S_n(f)} \propto \sqrt{\frac{P_n(f)}{R(f)}} \tag{13}$$

which corroborates the earlier definition.

Strain Sensitivity

The final strain sensitivity is defined as $h_{sys} = \sqrt{fS_n(f)}$, following the previous discussion and equation number (12). Considering the shot noise and acceleration noise we can write

$$S_n(f) = \left(\frac{P_{shot}+P_{OPN}}{D^2} + \frac{P_{acc}}{(2\pi f)^4 D^2}\right)/\mathcal{R} \tag{14}$$

NOISE BUDGET

We are to make an estimate for different noises that can disturb the interference pattern and may mask the effect of the gravitational waves on it. Here we follow the noise estimation for LISA made for single spacecraft. The main contribution comes from various types of acceleration noises generated by internal and external residual forces and the optical-path length noises produced by laser trap instabilities.

Here we have assumed N number of mirrors are working as sub-apertures of the primary mirror and those are connected to the optically tweezed element having damping coefficient k.

Acceleration noise

The main source of acceleration noise is the interaction between the fluctuating of Interplanetary Magnetic Field (IMF) and the spacecraft's own magnetic field, as well as the charged mirror bodies. These effects are unavoidable in space and therefore they need to be well-estimated in order to predict the noise floor. Other than these effects, forces generated by thermal distortions and residual gas pressures are also important components of this segment. Here we make an estimation of these forces using the available data of LISA path-finder and the predictive magnetic noise model by J.P.L. Zaragoza.

Magnetic Noise Calculation

The most prevalent magnetic noises comes from the interaction between IMF and different magnetic substances of the system, as well as the accumulated charges on the moving spacecrafts. The acceleration noise generated by the first effect is designated as Δg_{IMF}, whereas the second type of noise is due to the Lorentz force and hence marked as Δg_L. There may be some other spurious effects too, but those will not be as important as these two effects.

If we consider the interplanetary magnetic field (IMF) is aligned with x-axis, then the major components of the derived forces will be in that direction only. Now, the magnetic force along x-axis can be expressed as

$$F_x = \langle\left(\overrightarrow{M_r}.\vec{\nabla}B_x\right) + \frac{\chi}{\mu_0}\left(\vec{B}.\vec{\nabla}B_x\right)\rangle V \tag{15}$$

Therefore, the fluctuating force component can be written as

$$\delta F_x = V\left(\overrightarrow{M_r}\delta\vec{\nabla}B_x\right) + \frac{\chi V}{\mu_0}\left(\delta\vec{B}.\vec{\nabla}B_x\right) + \frac{\chi V}{\mu_0}\left(\vec{B}.\delta\vec{\nabla}B_x\right) \tag{16}$$

Where, $\chi = 10^{-6}$ is the magnetic susceptibility of the mirror, $\mu_0(= 4\pi \times 10^{-7}H/m)$ is magnetic permeability of vacuum and V is the volume of the detector, which is a constant term. This gives $(\chi/\mu_0)\sim 0.8m/H$.

M_r is the remnant magnetic moment of the material. For the mirror arrangments $|M_r| \sim 0.85\ nA\ m^2$.

This gives the relative acceleration due to the magnetic noise as

$$\Delta g_{IMF} = (\delta F_x)/\rho = \frac{V}{\rho}\left(\overrightarrow{M_r}\delta\vec{\nabla}B_x\right) + \frac{\chi V}{\mu_{0\rho}}\left(\delta\vec{B}.\vec{\nabla}B_x\right) + \frac{\chi V}{\mu_{0\rho}}\left(\vec{B}.\delta\vec{\nabla}B_x\right) \tag{17}$$

Now, from Zaragoza's work we can make an estimate of the IMF in the high frequency range, which is of our interest.

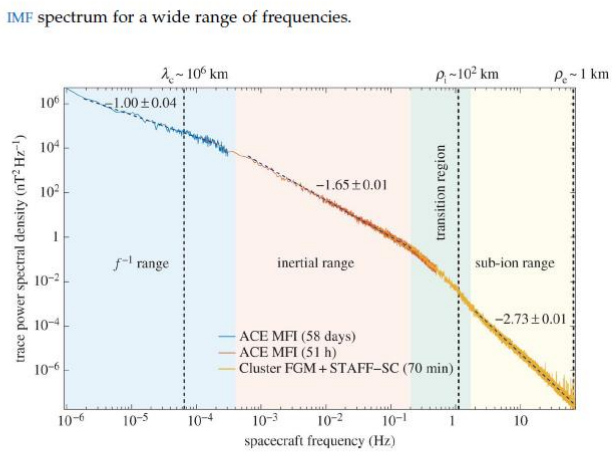

Figure 4. IMF spectrum for low to high frequencies. Curve taken from Zaragoza's work

In low frequency range the IMF spectral density follows 1/f variation, whereas for mid-frequency range (10^{-4} to 1 Hz) it follows $f^{-5/3}$ scaling and for higher frequencies, i.e. for more than 1 Hz, this follows $f^{-7/3}$ scaling. At high frequency region the magnetic field densities were not directly measured by LISA path finder, but it has been predicted by Zaragoza in his thesis. Here we use that fitted plot for our calculations.

5 MAGNETIC NOISE CONTRIBUTION TO Δg

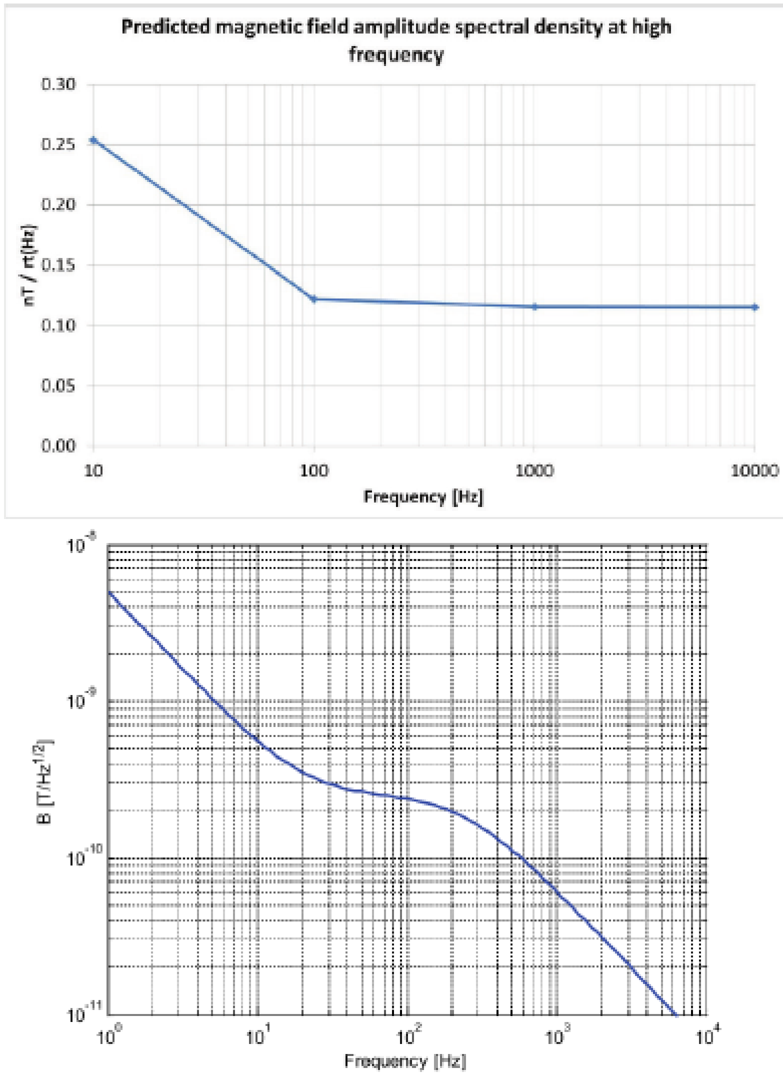

Figure 5. Predictive spectral densities for magnetic field at high-frequency region: Curve taken from Zaragoza's work

From the plot, we consider for ~20Hz, $B \approx 0.2\, nT$ and $\frac{\partial B}{\partial x} \approx 0.002 nT/m$.

Therefore, the first two terms of the relative acceleration functions evaluate as $|\overrightarrow{M_r}\delta\vec{\nabla}B_x| \sim 1 \times 10^{-21}$SI unit, and $\frac{\chi}{\mu_0}(\delta\vec{B}.\vec{\nabla}B_x) \sim 1 \times 10^{-18}$ SI unit. And the last term becomes $\frac{\chi}{\mu_0}(\delta\vec{B}.\vec{\nabla}B_x) \sim 1 \times 10^{-24}$ m/s²/√Hz,

Therefore, the net maximum relative acceleration

$$\Delta g = \sqrt{(1 \times 10^{-21})^2 + (1 \times 10^{-18})^2 + (3 \times 10^{-24})^2} \cong 1 \times 10^{-18} \text{ m/s}^2/\sqrt{\text{Hz}} \tag{18}$$

Thus, the acceleration noise due to fluctuating IMF will be in the range $1 \times 10^{-18} ms^{-2}/\sqrt{Hz}$

Lorentz force estimation:

The other most important magnetic interaction takes place between the IMF and the mirror arrangements on which electrical charges get accumulated. This results in an additional acceleration noise in the signal.

If the mirror arrangement or the spacecraft acquires a charge density q, and moves with a velocity $\vec{v}$ within IMF, then the Lorentz force on the body with volume V can be expressed as

$$\vec{F}_L = qV\langle\vec{E} + \vec{v} \times \vec{B}\rangle \tag{19}$$

Considering no spurious change in velocity may occur, we can write

$$\delta\vec{F}_L = V\delta q\, \vec{v} \times \vec{B} + Vq\, \vec{v} \times \delta\vec{B} \tag{20}$$

Now, from LISA pre-phase report, in this high frequency range, average charge accumulation per second is $q{\sim}2 \times 10^{-10}C$.

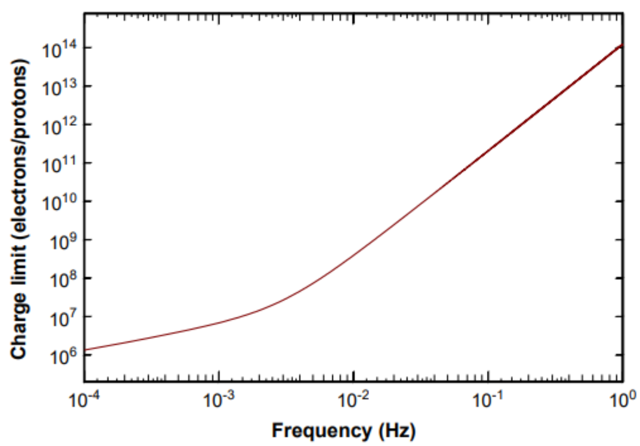

Figure 6. Ref: LISA pre-phase A

Therefore, keeping Hypertelescope integrating time in mind (for 500km it is ~0.0017s) we can safely use $\delta q{\sim}1 \times 10^{-10}C/s$. Again, for $B{\sim}2 \times 10^{-10}T$ and $\delta B{\sim}1 \times 10^{-11}T/s$.

$$\Delta g_L = \frac{\delta F_L}{\rho} \sim \frac{V}{\rho}\ 1 \times 10^{-21} ms^{-2}/\sqrt{Hz} \tag{21}$$

Other Effective Acceleration Noises:

The above-mentioned acceleration noises are unavoidable for a space borne system because of the presence of IMF and energetic particles in space. But, there are other noises too, which should be properly estimated and handled. Among those, noise generated due to thermal distortions of mirrors and spacecrafts and the self-gravity noises generated by such structural deformations are of main interest. However, those noises can be kept under control by careful design. In case of Hypertelescope, the deformations due to high power laser beam is very much less likely, but still we should keep the possibility in mind and design accordingly to keep it within the limit. Considering all the mirrors and three spacecrafts are experiencing these noises, we enlist the possible noise components in Table 1.

Table1. Acceleration noise

(Ref: LISA Pre-Phase A Report July 1998)

Description of Group	**Error Source**	**Acceleration @ 1-100Hz [$10^{-18}ms^{-2}/\sqrt{Hz}$]**	**Total Number of Effects affecting the interference**	**Sum of group (rms) for N=100, k=5e-7 [$10^{-18}ms^{-2}/\sqrt{Hz}$]**
External effects directly acting on the mirrors and space crafts	Magnetic force due to fluctuating interplanetary field	1.00	N	10
do	Lorentz force on charged bodies from fluctuating interplanetary field	1.00	N	10
Internally generated acceleration	Noise due to dielectric losses	1.00	N	10
do	Electrical force on charged bodies	1.00	N	10
do	Residual gas impacts on mirrors	1.00	N	10
Gravitational effect due to thermally induced mass distortion	Thermal distortion of mirrors	1.00	N	10
do	Thermal distortion of pay-loads	1.00	N.k	5
Contributor to residual acceleration resulting from control loop action	Gravity noise due to spacecraft displacement	1.00	3	1.73
Other substantial effects		0.50	(N+3)	5.15
Other smaller effects		0.30	(N+3)	3.10
Total effect of acceleration				73.98

Optical Path Noises

The optical path noises P_{OPN} will arise mainly from the positional uncertainty incorporated in the sub-aperture mirrors due to the laser noises, which will be used to trap the mirror carrying structures. A damped effect of laser phase and pointing noise will be propagated to the mirrors through the connectors having a damping factor k.

For our current calculation we consider the best-known values for laser noise, given in terms of Relative Intensity noise (RIN) ~ -160dB/Hz which is equivalent to the power ratio $1 \times 10^{-16}/Hz$ reported by LP2N group in 2022 for their tunable high power MOPA laser. This power ratio equals the path length noise to path length offset (DC readout) ratio, i.e. the steady path-length offset value multiplied by this RIN will determine the noise floor of the optical path noise. Therefore, we can safely expect the noise power floor to be in the range $1 \times 10^{-16} m^2/Hz$. This noise will be damped by connector's damping factor. The value of damping factor has been collected from LIGO's four-stage damping. A list of effects is given in Table2. All the noises must be scaled by the laser noise and damping factor and added quadratically to get the noise power in m^2/Hz unit (Robson et. al., 2019).

Table2. Optical Path noises

Error Source	**Effect per path**	**Number of paths**	**Sum of group (rms) for N=100, scale factor = $\mathbf{2 \times 10^{-16} m/\sqrt{Hz}}$ and k=5e-7**
Master Clock Noise	1	1	$1 \times k$
Residual laser phase noise after correction	1	2N	$20 \times k$
Laser phase measurement and offset lock	1	2	$1.4 \times k$
Laser beam pointing instability	1	2N	$20 \times k$
Scattered-light effects	1	N+1	10.1
Other substantial effects	3	N+1	30.3

DISCUSSION: FINAL SENSITIVITY OF THE SYSTEM

Now with these budgeted values of acceleration noises and optical path noises in hand and following equation (14), we achieve the strain sensitivity curve as follows:

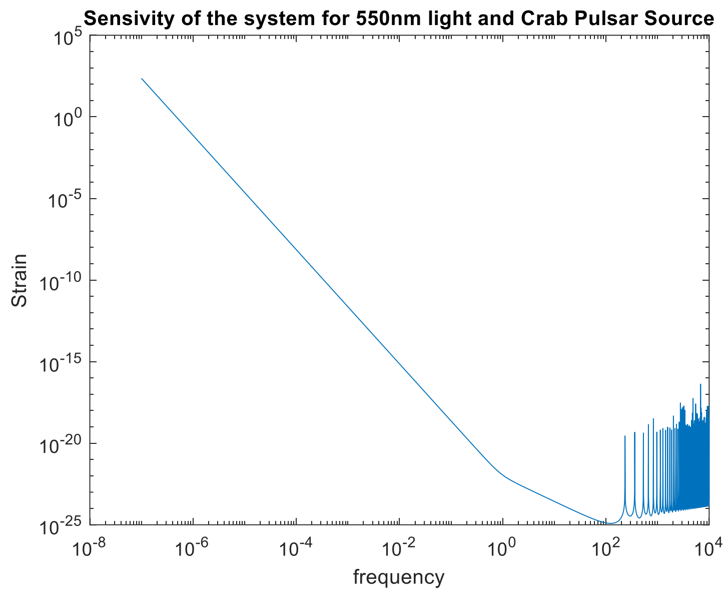

Figure 7. Sensitivity of Space based Hypertelescope array spanning over 1000km

This shows the system will be sensitive to the gravitational wave for high frequency range, i.e. for frequencies more than 1Hz. Here, it should be noted that this strain sensitivity has been calculated from the cumulative phase differences created by the mirror array displacements at detector, but detector's efficiency has not been considered. Therefore, finally the sensitivity will depend upon that factor, but cannot go beyond this curve.

Thus, Hypertelescope array with 1000km baseline, at its maximum capacity will be able to detect the effect of Compact Binary Inspiral, Core Collapse Supernovae, Pulsars and GW150914.

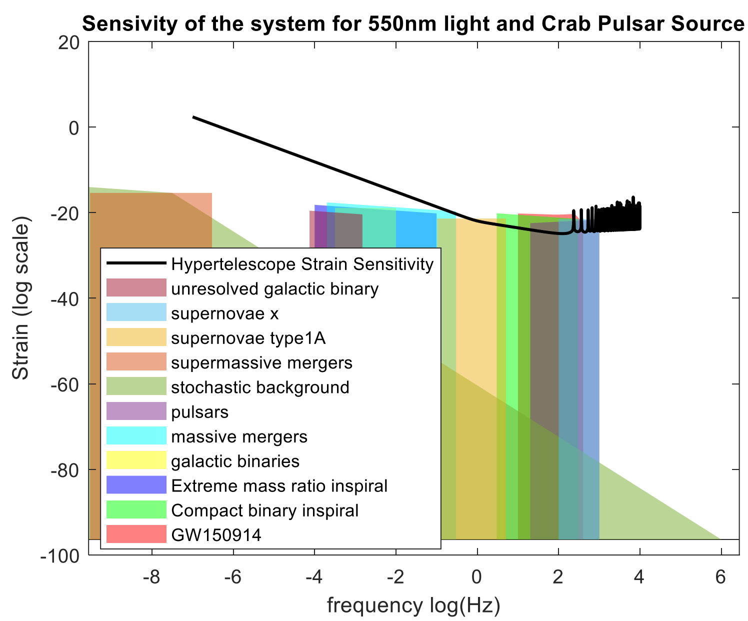

Figure 8. Hypertelescope sensitivity curve. The data for strains generated by various sources was collected from gwplotter website

CONCLUSION

In this present communication, we have suggested some structural modifications for the space-hypertelescope, in order to make it a gravitational wave detector besides a high-resolution direct-imaging telescope. The proposed three-satellite structure will be able to detect the gravitational waves produced by various supernovae, mergers, pulsars, and compact binary inspirals, which have frequencies around and above 1Hz. This range of detection is estimated for 1000km configuration of the primary mirror array – in order to achieve sufficient photons from the targeted celestial object, we have to put this constraint over its span. If the targeted source be brighter, we may construct the primary mirror base line even longer, which will make the system sensitive to gravitational waves with further lower frequency range. A detection system with super-resolution will be helpful to detect the fringe variations due to mirror displacements, and for effective use of such a system a brighter celestial object rendering ample photon flux will be beneficial.

REFERENCES

1. Park, I.H., Kim, D.H., Choi, K.-Y. & Won, E. 2019
2. Park, I.H., Choi, K.-Y., Hwang, J., Jung, S., Kim, D.H., Kim, M.H., Lee, C.-H., Lee, K.H., Oh, J.J., Oh, S.H., Park, M.-G., Park, S.C., Pozanenko, A., Rho, C.D., Vedenkin, N. & Won, E. 2020
3. Park,I. H. 2021, Journal of the Korean Physical Society 78, 886–891, https://doi.org/10.1007/s40042-021-00118-x
4. Labeyrie, A. 1996, Astron. Astrophys. Suppl. Ser. 118, 517-524
5. Labeyrie, A. 2018, Multi-Pixel Imaging of Exoplanets with a Hypertelescope in Space in Handbook of Exoplanets ed Deeg, H. J. & Belmonte, J. A., (Springer International Publishing AG) https://doi.org/10.1007/978-3-319-55333-7_168
6. Zheludev, N. I. & Yuan, G. (2022). Optical superoscillation technologies beyond the diffraction limit. Nature Reviews Physics, 4, 16-32. https://dx.doi.org/10.1038/s42254-021-00382-7
7. Katrine S. Rogers, Konstantinos N. Bourdakos, Guang Hui Yuan, Sumeet Mahajan, and Edward T. F. Rogers, "Optimising superoscillatory spots for far-field super-resolution imaging," Opt. Express 26, 8095-8112 (2018)
8. http://www.vikdhillon.staff.shef.ac.uk/teaching/phy217/instruments/phy217_inst_photsys.html#table1
9. Carroll, S. 2004, Spacetime and Geometry (An Introduction to General Relativity, Pearson, San Francisco)
10. https://brilliant.org/wiki/gravitational-waves/
11. Robson, T., Cornish, N.J. & Liu, C. 2019 *Class. Quantum Grav.* **36,** 105011 https://doi.org/10.1088/1361-6382/ab1101
12. Moore, C.J., Cole, R.H. & Berry, C.P.L. 2015, Class. Quantum Grav. 32, 015014 doi:10.1088/0264-9381/32/1/015014\
13. http://gwplotter.com
14. J.P.L. Zaragoza, ‘Magnetically induced forces during LISA pathfinder in-flight operations’, Ph.D. thesis, Barcelona, 2020
15. LISA Pathfinder, Pre-Phase A Report, July 1998

16. D. Darwich, R. Prakash, C. Dixneuf, Y.V. Bardin, M. Goeppner, G. Guiraud, N. Traynor, G. Santarelli and A. Hilico, 2022, Opt Express 30, 12867-12877 https://doi.org/10.1364/OE.455218

17. A Labeyrie, HL Coroller, S Residori, U Bortolozzo, Pathways Towards Habitable Planets, 2010, https://scholar.google.com/citations?view_op=view_citation&hl=en&user=KptxDG0AAAAJ&cstart=20&pagesize=80&sortby=pubdate&citation_for_view=KptxDG0AAAAJ:ZHo1McVdvXMC

18. A. Labeyrie, P. Riaud, S. Residori, U. Bortolozzo, F. Vakili. Proposition soumise à l'Agence Spatiale Européenne le 24 Mai 2013, chrome-extension://efaidnbmnnnibpcajpcglclefindmkaj/https://projets.oca.eu/images/LISE/pdf_publications/WhitepaperProposalHypertelescope.pdf